Research Article Vol. 3, No. 12 / December 2016 / Optica 1285

Stress-state manipulation in fused silica via femtosecond laser irradiation

Yves Bellouard,[1,2,*] Audrey Champion,[2] Benjamin McMillen,[1,2] Sebabrata Mukherjee,[3] Robert R. Thomson,[3] Charles Pépin,[4] Philippe Gillet,[4] and Ya Cheng[5]

[1]Galatea Lab, STI/IMT, Ecole Polytechnique Fédérale de Lausanne (EPFL), 2002 Neuchâtel, Switzerland
[2]Mechanical Engineering Department, Eindhoven University of Technology, 5600 MB Eindhoven, The Netherlands
[3]Institute of Photonics and Quantum Sciences, Heriot-Watt University, Edinburgh EH14 4AS, UK
[4]Earth and Planetary Science Laboratory, IPHYS/SB, Ecole Polytechnnique Fédérale de Lausanne (EPFL), 1015 Lausanne, Switzerland
[5]Shanghai Institute of Optics and Fine Mechanics, Chinese Academy of Sciences, Shanghai 201800, China
*Corresponding author: yves@bellouard.eu

Received 2 May 2016; revised 15 September 2016; accepted 18 September 2016 (Doc. ID 264400); published 7 November 2016

Controlling the stress in glass after laser exposure is of prime importance not only for photonics applications, but also for preserving the mechanical integrity of glass components in general. The sub-surface exposure of fused silica to femtosecond laser pulses can induce a permanent and localized modification to the glass structure. In this work, we present evidence that femtosecond laser exposure can be used to continuously tailor the stress in the material, from a tensile to compressive state, as the laser pulse energy is changed. In addition, we demonstrate that this effect can not only be obtained while transitioning between different laser-induced microstructures, but also at low pulse energy, in the laser exposure regime particularly relevant for fabricating waveguides. These results demonstrate that femtosecond laser exposure is a versatile tool for fully controlling the stress landscape in a volume of silica, opening up new technological opportunities, like for instance, direct write stress-free waveguides, direct-write stress-induced birefringence state or mechanically reinforced parts, by locally preloading it.

OCIS codes: (160.2750) Glass and other amorphous materials; (160.6030) Silica; (320.2250) Femtosecond phenomena; (320.7130) Ultrafast processes in condensed matter, including semiconductors.
http://dx.doi.org/10.1364/OPTICA.3.001285

1. INTRODUCTION

The exposure of dielectric materials to ultrashort laser pulses leads to a radically different laser–matter interaction than that observed for longer pulses [1–4]. In particular, ultrashort laser pulses can be used to induce highly localized structural changes that have different physical properties from that of the unexposed material. This capability has emerged as a versatile tool for the direct-write fabrication of a variety of devices, finding applications as diverse as integrated photonics [5–10], novel optical components [11,12], optofluidics [13–16], micromolding [17,18], optomechanics [19], microactuators [20,21], micromechanics [22], material testing [23], and electro-optics [24].

In the case of fused silica, different types of structural modification can be induced. The exact form of this modification is a function of the laser writing parameters, including the pulse energy, duration, and repetition rate. When structures are fabricated using pulse durations of approximatively 200 fs, and pulse repetition frequencies that are sufficiently low to avoid cumulative heating effects [25] (i.e., the laser interaction is essentially athermal), two laser-induced morphology regimes are found. In the first regime, commonly referred to as "Type I" in the literature [5], when using low pulse energies, a smoothly varying structural modification is observed in and around the region where the focused instantaneous power exceeds a first threshold of intensity [26]. A second regime is accessed by increasing the pulse energy above a second threshold intensity. In this second regime (referred to as "Type II"), it is found that the modified region consists of self-organized nanostructures—commonly referred to as nanogratings [27].

While various models have been proposed [27–30] to explain the formation of nanogratings, the exact nature of their formation remains elusive. Interestingly, it has been shown that the morphology can be controlled by changing the pulse duration and/or the pulse energy [31,32]. Thus far, however, little attention has been paid to the volumetric changes associated with the morphological transition between the two types of structures, and more generally, to the stress associated with laser-induced structural changes.

On one hand, it has been shown that an increase of refractive index is associated with Type I modifications [5], and that this increase in refractive index can be correlated to material

densification using nanoindentation and digital holographic microscopy (DHM) [33], suggesting a localized reduction of volume. The most likely densification mechanism, supported by Raman observations [32,34], is the formation of rings of order three (corresponding to a D2-peak increase in Raman spectra). On the other hand, the second regime exhibits a net volume expansion, as recently shown in [35]. This net volume expansion can be correlated to the formation of porous structures inside the nanogratings, as reported in [36,37]. This volume expansion further leads to stress that depends on the orientation of the writing polarization [38,39] that controls the nanograting orientation. For instance, linear laser polarization produces nanoplanes parallel to one another and aligned perpendicular to the laser polarization direction [27]. More exotic polarization states, such as azimuthal or radial, produce more complex—yet self-organized—structures, such as star shapes, concentric circles, or mixtures of domains [40,41].

Recent observations [42] have shown the existence of different stress states as a function of the pulse duration, and therefore as a function of the laser-induced morphologies. In addition, hints [43] suggest that the exposure dose (or "energy deposited") may also play a significant role in the laser-induced stress in the material.

Here, we investigate how induced stress varies as a function of laser exposure parameters, in particular during the transition between Type I and Type II regimes, but also as a function of energy deposition. Understanding these material modifications and the associated stress states are key elements required to unravel the mechanisms underlying sub-surface structural modifications in silica glass. Furthermore, the proposed methodology presented here is rather generic. It can inspire other studies dedicated to other material systems exposed to femtosecond lasers.

2. METHODOLOGY

A. Cantilevers as a Probe of Internal Stress

To investigate laser-induced stress states, we used a method based on microcantilevers, which is explained in detail elsewhere [35]. Since this method plays a key role in the observations reported here, we briefly outline its main features. The working principle (illustrated in Fig. 1) is to use an elongated-cantilever femtosecond laser fabricated from glass using the process described in [44]. Following fabrication, the cantilevers are exposed to focused femtosecond laser pulses, but the layer of exposure is maintained at a depth of 15 μm and close to the cantilever anchoring point. Previous studies using surface profiling techniques indicated that this was sufficient to avoid surface modifications (either ablative or undulations on the surface). The modified/unmodified areas define a composite bimorph, such that a change of volume in the laser-affected zone will bend the cantilever either up or down, depending on the sign of the volume change. Since the net laser-induced volume variations are small, the cantilevers were intentionally fabricated long to mechanically amplify these deformations into a measurable displacement at the end of the beam. Using this measurement and Stoney's equation [45], we extract the equivalent average deformation in the laser-affected zones, as well as the corresponding average stress of the laser-affected zones. We highlight the fact that the laser-affected zones, in particular in the second regime, are known to be composite structures that include nanobubbles, nanogratings, and other nanoscale features.

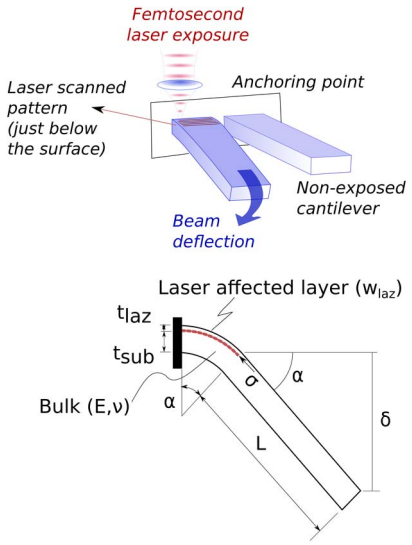

Fig. 1. Illustration of the cantilever-based methodology used to accurately measure volume variations induced by femtosecond laser exposure. The cantilever devices are exposed to a focused femtosecond beam near the top surface (approximatively at a depth of 15 μm), using a series of closely spaced (~2 μm spacing) parallel lines.

As such, the cantilever method would not indicate any local variations at the composite scale, i.e., at a micrometer scale, but rather an average stress measurement over the full laser-modified layer. We have shown in previous work [35] that this analytical model provides an accurate measurement of the average strain.

In these experiments, the laser polarization was linear, and set either parallel or perpendicular to the laser writing direction. The average strain and average stress are given by, respectively,

$$\epsilon_{\mathrm{avg}}(\delta) \approx \left(\frac{t_{\mathrm{sub}}}{2w_{\mathrm{laz}}}\right)\frac{\delta}{L}, \qquad \sigma_{xx}(\delta) \approx \left[\frac{Et_{\mathrm{sub}}^2}{6w_{\mathrm{laz}}(1-\nu^2)t_{\mathrm{laz}}}\right]\frac{\delta}{L}, \quad (1)$$

where t_{sub} is the thickness of the cantilever, t_{laz} is the thickness of the laser-affected zone, w_{laz} the width of the laser exposed area in a direction perpendicular to the cantilever, δ is the deflection of the cantilever, ν the Poisson ratio, L the length of the cantilever (measured from the end of the laser-affected section to the tip of the beam; see Fig. 1), and E is Young's modulus of the silica substrate. The ratio δ over L effectively accounts for the amplification factor that can be tuned as needed.

The expression above is valid under the assumption that the thickness of the substrate is much bigger than the thickness of the laser-affected layer (i.e., $t_{\mathrm{sub}} \gg t_{\mathrm{laz}}$). Note that a more rigorous expression for the average strain when this condition is not fulfilled can be derived from the bimorph analysis derived by Timoshenko [46]. Furthermore, the expression above gives an estimate of the average strain and stress considering a homogenized layer. In reality, the laser-affected zone is created by writing a set of parallel lines with a given density (here every two micrometers) (Fig. 2). The width (along X) and thickness (along Z) of each laser-affected zone depends on the pulse energy, and to a lesser extent on the energy deposited.

The effective strain is deduced from the average strain as follows. Since the cantilever is free at one end, and the shape of the laser-affected zones is such that its $Z_0 > X_0$, we can assume that the average strain is simply the product of the number of lines

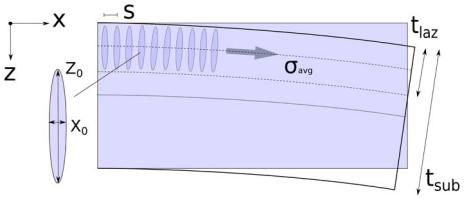

Fig. 2. Schematic of the cross section of a cantilever with laser-affected zones (shown in the case of a volume expansion). The laser-affected layer consists of a series of lines, each spaced by a distance s from its neighbor and written parallel to one another across the width of the cantilever. Considering the moderate numerical aperture used in these experiments, the cross section of the laser-affected zone has the shape of an elongated ellipse, with X_0 and Y_0 as short and long axes, respectively.

multiplied by the width (X_0) of a laser-affected zone that has densified or expanded after exposure. For the regime where low fluences are used (which will be the case here), the shape of the laser-affected domain boundary can be approximated by an ellipse whose short and long axes depend on laser pulse intensity, and can be derived by adopting a simple model based on threshold intensity to capture the nonlinear absorption domain (see Appendix A for the derivation of the expressions). Using this formalism, X_0 and Z_0 are

$$z_0(I) = 2\left(\frac{\pi n w_0^2}{\lambda}\right)\sqrt{\left(\frac{I_0}{I} - 1\right)}, \quad x_0(I) = 2\sqrt{\frac{w_0^2}{2}\log\left(\frac{I}{I_0}\right)}, \tag{2}$$

in which I is the focused peak intensity, I_0 the threshold intensity for nonlinear absorption, n the refractive index of the media, λ the wavelength of the laser, and w_0 the beam waist at the focus. By using Eqs. (1) and (2), the effective strain in the laser-affected zones can be deduced from the average strain itself calculated from the cantilever defection measurements, derived in Eq. (1), through a proportional relation:

$$\epsilon_{laz} = \left(\frac{w_{laz}}{n_{lines} X_0}\right)\epsilon_{avg}. \tag{3}$$

Here, w_{laz} is the total width of the laser-affected zone, X_0 the width of a single laser-affected zone [calculated using Eq. (2)], n_{lines} the number of written lines, and ϵ_{avg} the average strain calculated from Eq. (1).

B. Experimental Details: Lasers and Instruments Used

For the work presented here, we used two lasers. The first was a Yb-based regenerative amplifier (from Amplitude Systèmes), delivering 150 fs pulses at a wavelength of 1030 nm and pulse repetition frequency of 100 kHz. The second was a Yb-doped fiber amplified system (Amplitude Systèmes, 380 fs, here used at a repetition rate of 800 kHz). According to the work from Hnatovsky *et al.* [31], the 150 fs pulses generated by the regenerative amplifier lie within the region where both Type I and Type II structures can be attained through control of the pulse energy (note that this observation was also confirmed in [32]). The laser-affected zones consist of lines produced by translating fused silica substrates (high OH content, >1000 ppm) through a fixed laser focus using linear translation stages (PI-MICOS). The focus was formed with a 0.4 NA objective (Thorlabs, LMH-20X-1064) producing a focal spot diameter of ~1.5 μm. Substrate translation speeds were varied from a few micrometers per second to tens of millimeters per second. The cantilever displacement was measured using a digital holographic microscope (DHM, Lyncee Tec), which provides nanometer accuracy. The cantilevers used in these experiments are themselves produced using the Yb-fiber laser according the process described in [44].

To provide additional insight into the nature of the laser modification, a second set of modifications were inscribed into an un-modified silica substrate, using exactly the same exposure conditions used for inscribing structures on the cantilevers. Following inscription, the substrate was edge polished to reveal the cross sections of the inscribed modifications, in preparation for investigation using scanning electron microscopy. Prior to SEM observation, the substrate was briefly etched (<5 min) in a low-concentration bath of hydrofluoric (HF) acid to reveal any microstructure within the laser-affected zones.

To further correlate the optical properties of the inscribed structures with the stress state of the material, laser-written lines were arranged to form waveguides with an approximately rectangular cross section [47–49]. The guided modes of these structures were subsequently investigated by coupling 633 nm light into one end of the structure while imaging the output facet onto a CCD camera. Propagation losses of the inscribed structures were measured by coupling 633 nm light into the structure under test and measuring the decay of the scattered light intensity along the waveguide [50]. An exponential decay was observed along the propagation direction, as would be expected for a waveguide with a homogeneous propagation loss profile. The loss coefficient for each waveguide was then evaluated by fitting an exponential function to the imaged intensity profile.

3. RESULTS AND DISCUSSION

A. Cantilever Beam Deflection as a Function of Pulse Energy

In a first set of experiments, a series of cantilevers were modified, where the pulse energy used for each cantilever was gradually increased from the threshold for modification up to the ablation threshold. The results from the cantilever experiments using these parameters are shown in Fig. 3. Two regimes are immediately identifiable for both laser polarizations, denoted by areas in each panel of the figure.

In the first regime, the cantilever deflects upward, clearly indicating an overall volume reduction in the laser-affected zone and, therefore, a localized densification. Here, the maximum upward deflection peak corresponds to an equivalent average tensile stress of about 40 MPa, which is relatively modest. The densification of the SiO_2 matrix is related to the formation of metastable three-ordered rings (note that observations of the increase D2 peak in the Raman spectra of laser-affected zones support this hypothesis [32]).

In the second regime, a downward deflection is observed, with an absolute magnitude that is larger than that found for the first regime, and corresponding to a net volume expansion of the laser-modified zones. While the overall behavior is the same for both polarization states, there are noticeable differences between the two cases. In particular, the transition between the two stress states occurs at a lower pulse energy when the laser polarization

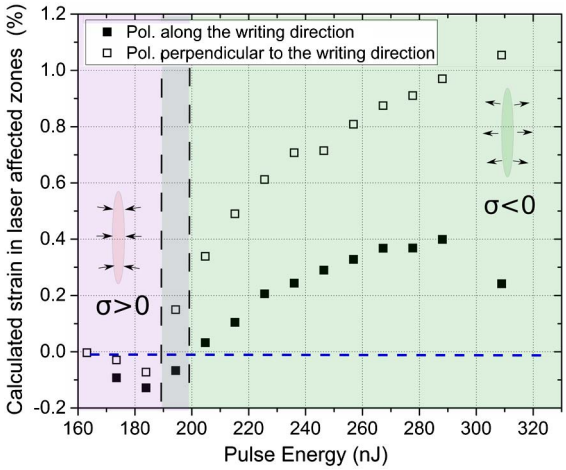

Fig. 3. Measurements of cantilever deflection after exposure to 150 fs laser pulses for increasing energy per pulse for both polarizations. The writing speed was fixed at 4.8 mm/s (repetition rate of 100 kHz). The estimated relative error on the calculated strain from the measurement is in the range of 10%. The measurement error on the pulse energy measurement is ±5 nJ.

is oriented perpendicular to the exposed lines' axis (itself oriented parallel to the long axis of the cantilever). Furthermore, when the writing polarization is oriented along the line direction, the amplitude of deflection in the second regime is much lower thanthat observed for the perpendicular polarization case.

It is also worth noting that, even at low energies, in the so-called "homogeneous" regime range, the amplitude of upward deflection is noticeably different for the two polarizations, suggesting that this first regime *also* exhibits a certain level of anisotropy, and that the usual classification of "homogeneous" for this regime is incorrect. Similar observations, this time on subtleties in the Raman spectra for both polarizations, were made in [32]. In this work, an increase in the D2 peak that to a certain extent can be correlated to an increase of silica rings of order three, were found to be more prominent in the case of longitudinal polarization than for the transverse polarization. This observation seems consistent with the experiment reported in Fig. 3. If a higher compaction takes place for longitudinal polarization, the amplitude of upward bending of the beam would increase, as observed.

We note that when reaching higher pulse energy (i.e., around 300 nJ), the strain may decrease (as can be seen in Fig. 3). We attribute this behavior to the occurrence of cracks, and consequent relaxation phenomena, due to the high level of stress in the cantilevers.

From these measurements, we can estimate the refractive index variation that would be expected from compaction, expansion, and polarizability changes. To do so, we consider the derivation of the Lorentz–Lorenz relation [51–53]:

$$\Delta n_\lambda = \left[\frac{(n_\lambda^2-1)(n_\lambda^2+2)}{6n_\lambda}\right]\left(\frac{\Delta\rho}{\rho}\right)(1+\Omega) \quad \text{with } \Omega = \left(\frac{\Delta\alpha}{\alpha}\right)\frac{\Delta\rho}{\rho}. \tag{4}$$

Here, n_λ is the refractive index at wavelength λ, α represents the polarizability, and ρ is the density. The term Ω is the product of relative polarizability change to relative density change. Considering that the densification is uniform across the laser-affected volume (this hypothesis is based on thermal conductivity measurements [32]), we can relate the uniaxial strain with the relative density variation by the following equation:

$$\left(\frac{\Delta\rho}{\rho}\right) \approx \left(\frac{3}{1+2\nu}\right)\epsilon_{\text{laz}}. \tag{5}$$

In this equation, ν is the Poisson coefficient and ϵ the linear strain for the laser-affected zones. Reference [53] measured Ω in the case of a UV laser densified to be about $-0.23 +/- 0.04$. The same reference aggregates data from other experiments achieved under a broad range of different densification means (from hot isostatic pressing to electron irradiation). The literature suggests that Ω varies typically from −0.15 to −0.22 for various types of beam exposure conditions, in particular for excimer laser UV exposure that resembles, to a certain extent, our exposure conditions. Here, for a first estimate of the refractive index increase, we use these values in the case of the highest measured densification in the case of Fig. 3 (the relative error corresponds to the span of possible values for Ω):

$$\Delta n_{\parallel} = 0.000121 \pm 0.000006, \quad \Delta n_{\perp} = 0.000069 \pm 0.000003.$$

This demonstrates that this experimental technique can also potentially be used for estimating index variations *without* any optical means and/or dependence on optical properties of the waveguide itself. In the estimate above, we have considered that the laser-modified zones were homogeneous (as it is commonly assumed in the literature for the first regime). The fact that refractive index values differ from the two polarizations suggest one more time that there exists a certain level of anisotropy also in Type I modifications.

B. Scanning Electron Microscope Cross-Section Observations

Insight into the transition from one stress state to another can be gained by careful study of the morphological changes found in the laser-affected zone as the pulse energy is increased. With this in mind, lines were again inscribed with the same exposure conditions used for the cantilevers, concentrating on the pulse energy range where the transition between tensile and compressive stress is observed. The sample was then sectioned, polished, and briefly etched before analysis using a scanning electron microscope (SEM). Since nanogratings are believed to be the underlying mechanism behind these stress states, observations were conducted only on specimens exposed with the laser polarization perpendicular to the writing direction, ensuring that the nanogratings are oriented properly for observation in the SEM. These observations, shown in Fig. 4, are particularly interesting, as a gradual transition between "continuous" and self-organized structure is observed.

Nanogratings begin to appear near a pulse energy correlated with the transition between stress states (in these experiments, between 170 and 190 nJ for nanograting formation, while the stress-state transition was observed around 185 nJ). This supports recent observations reported in [36,37] that demonstrated that nanogratings contain porous media, possibly originating from a decomposition of the glass matrix and the formation of molecular oxygen. To test this hypothesis, we performed Raman observations (shown In Fig. 5) of specimens written with 300 nJ pulses, i.e., well in the exposure regime where nanogratings are forming.

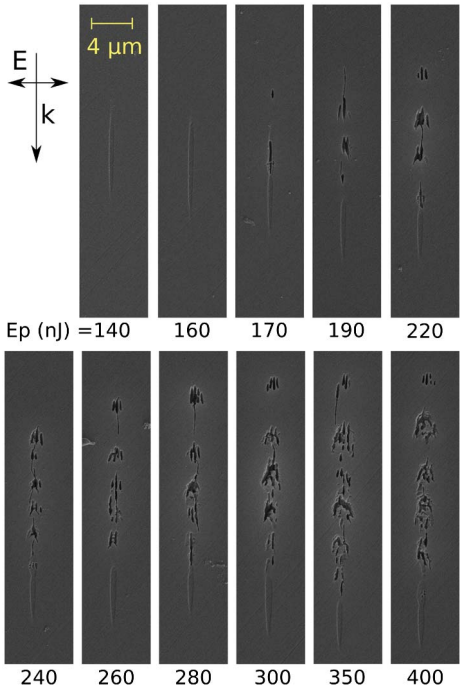

Fig. 4. Evolution of the morphology of individual laser-modified zones with increasing pulse energy (writing speed was set to 4.8 mm/s, repetition rate is 100 kHz). These SEM images were obtained by observing the cross section of a polished silica substrate containing laser-written lines.

The Raman spectra reveal, in addition to the expected increase in the D2 peak at around 600 cm^{-1} [32], the development of two new peaks at 1549 and 1556 cm^{-1}, which are due to the presence of molecular oxygen, validating the glass matrix decomposition when nanogratings form [37].

It is logical to associate the formation of these nanopores with a volume expansion and, consequently, compressive stress surrounding laser-affected zones. Equally interesting is the coincidence of nanogratings and a smoothly modified region in the transition zone between tensile and compressive regions (i.e., a region of "mixed" morphology). We explain these phenomena by first recalling that, in this work, a moderate numerical aperture

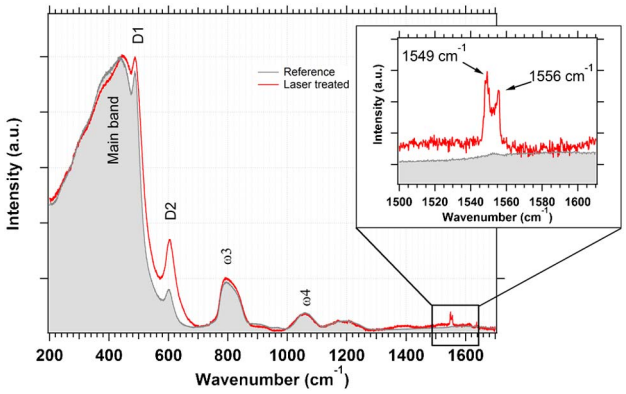

Fig. 5. Raman of the laser-affected zone at high pulse energy (in the nanograting regime) compared to a Raman spectra (dark gray) of the same glass in the region where it was not exposed to the laser. We note the presence of two new peaks at 1549 and 1556 cm^{-1}, corresponding, respectively, to dissolves O_2 in the silica network and to molecular O_2. Raman spectra are normalized using the band ω_4.

of 0.4 was used, which results in a focal volume with a confocal parameter of ~6 μm. Once the instantaneous energy density is sufficiently high, nanogratings form, eventually creating multiple foci (not necessarily periodic) owing to nonlinear self-focusing and plasma-induced defocusing along the propagation axis. The nanograting formation may be according to a mechanism proposed recently in [30] that involves laser-induced plasma wave formation at the interfaces of seed structures.

From these observations, correlations can be drawn between the intensity of the propagating laser field and the evolution of the grating morphology. For a given laser-affected zone (for example, at pulse energies above 190 nJ), as the pulse energy is gradually depleted during light propagation through the material, the grating periodicity changes according to this reduction in energy. This also suggests the existence of threshold field intensities for the production of periodic structures. Indeed, below 190 nJ in Fig. 4, no nanogratings are visible.

C. Effect of Deposited Energy in the Regime of Homogeneous Modification

Let us now consider the formation of nanogratings as a function of deposited energy (i.e., the number of pulses passing through a given cross section of material). Here, the pulse energy is fixed and chosen in a regime where nanogratings are formed. Taking the results shown in Fig. 4 as a reference, a pulse energy of 250 nJ was chosen. The amount of deposited energy was controlled by varying the translation speed of the substrate. In this manner, full control of the laser exposure fluence is possible, while maintaining the peak exposure intensity. The results of this experiment are shown in Fig. 6, where it can be seen that segmented nanograting zones gradually form at different depths, eventually connecting along the direction of light propagation as the deposited energy is increased.

These observations support previous models, which attempted to explain the formation of nanogratings through a localized field enhancement, known as the "nanoplasmonics" model [28–30].

To test whether nanograting formation is simply a consequence of deposited energy or subject to a threshold field intensity, an additional test was performed. Similar to the previous experiments, the deposited energy was again controlled by varying the translation speed, but with a lower pulse energy of 170 nJ, chosen to lie firmly within the first (or "homogeneous") modification regime. A cantilever-bending experiment (as described in Fig. 1) was conducted, and correlated to SEM observations of the cross

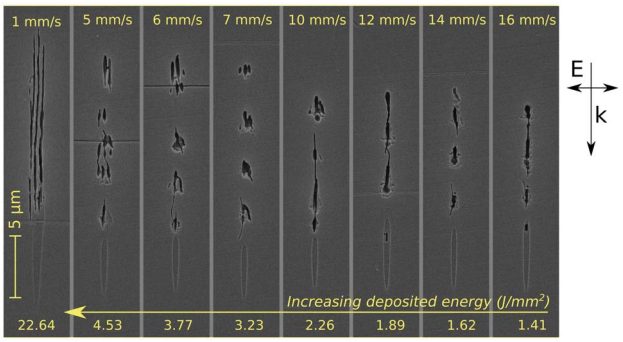

Fig. 6. Morphology of the laser-affected zone as a function of the deposited energy. Pulse energy was fixed at 250 nJ (delivered at 100 kHz), corresponding to a regime in which nanogratings are formed.

section of laser-affected zones for the same exposure parameters. The combined results are shown in Fig. 7, from which two important conclusions can be drawn. The first conclusion is that *no nanograting formation* is observed as the deposited energy is increased (i.e., fixed pulse energy, but progressively slower translation speed). Here, the laser-affected zone is found to expand along the optical axis, but with the absence of nanogratings. This information indicates that the pulse energy and, therefore, the field intensity for sub-200-fs pulse duration, is a key factor for triggering nanograting formation. This characteristic trait is possibly rooted in the requirement of a minimum electron density for excitation of nanoplasmonic waves, necessary for the initiation of the process of nanograting formation [28]. The expansion along the optical axis may be attributed to the increased refractive index that tends to shift up the focus as more pulses are gradually deposited in the material.

In these cantilever experiments, a stress-state inversion is also observed despite the absence of nanogratings. This fact suggests that the material produced in regime I is not homogeneous, and may consist of a composite structure, mixing nanopores and densified zones. This decomposition of the glass matrix and the formation of pores in the laser-affected zones, as described by Lancry *et al.* [37], results in a net volume expansion. *De facto*, two competing phenomena are present: one that leads to densification of the glass matrix (appearance of ring of shorter order as suggested by Raman observations) and the gradual decomposition of the glass matrix. The formation of such pores is therefore uncorrelated with the presence of nanogratings.

These two experiments (i.e., an increase of deposited energy for either fixed pulse energy or fixed scanning velocity) highlight the importance of the peak laser intensity and, therefore, the plasma density in the formation of self-organized nanogratings. This shows that their formation is governed by three parameters: pulse energy, pulse duration, and cumulatively deposited energy for a given (fixed) pulse energy.

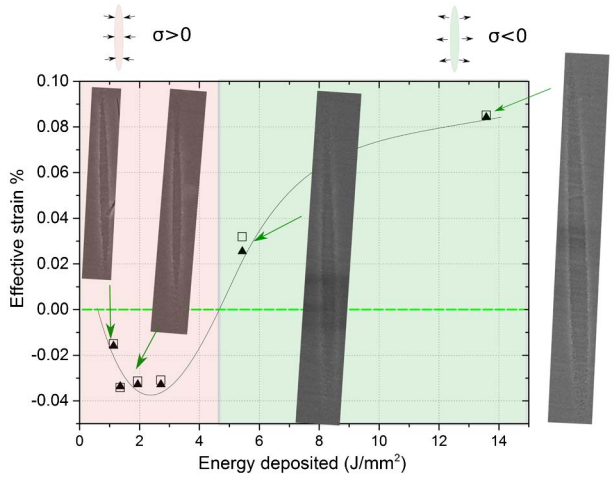

Fig. 7. Results of the cantilever bending experiment performed in the regime where no nanogratings are found. Here, the pulse energy was fixed at 160 nJ while gradually increasing the deposited energy by reducing the writing speed. Similar to the case of increasing pulse energy (see Fig. 2), an inversion of stress state is observed; however, in this case, there is no observable correlation with the formation of nanogratings. (Note: the trend is provided as a visual guide and does not represent a predictive model.) The laser polarization was perpendicular to the substrate translation direction.

To comprehend the role of pulse duration in the transition between continuous modifications and nanograting formation, using pulse duration of 270 fs (i.e., above the 200 fs threshold proposed by Hnatovsky *et al.* [31]), we conducted cantilever experiments, but this time with deposited energies kept as low as possible by increasing the scan speed. These experiments consistently yielded the same result, indicating an overall volume expansion but no overall densification regime (data not shown here). Note that these results are also consistent with the results reported in [31]. This suggests that the time duration of 200 fs is a critical time constant in the process of densification.

D. Waveguiding Properties as a Function of Energy Deposited

Lines inscribed using laser parameters that induce densification are known to guide light. To confirm this observation, four parallel lines were written, each spaced by one micrometer relative to the other, forming a waveguide with a nearly rectangular cross section. The pulse energy was set at 160 nJ, so as to be firmly in the tensile stress regime and with no mixing between different types of modification, as revealed in Fig. 3. The geometry of these waveguides is based on work described by Bado *et al.* [47,48]. SEM images of these waveguides are shown in Fig. 8 as well as measurements of the propagation losses.

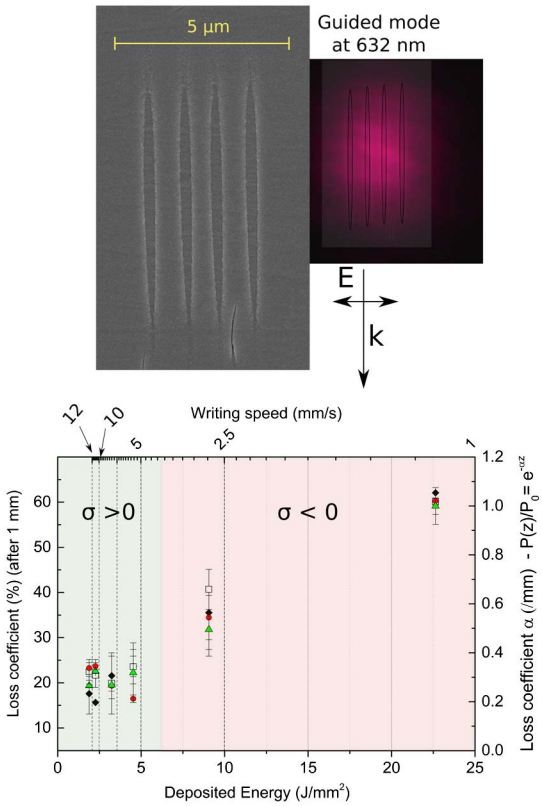

Fig. 8. Waveguide written in the first regime according the design from Bado *et al.* [47] Top: SEM cross section of a waveguide written at 10 mm/s. The inset shows the Gaussian guided mode at 632 nm. In this inset, the SEM picture is overlaid in transparency for reference. Bottom: waveguide propagation losses (measured according the method described in [50]) as a function of deposited energy and writing velocities. The various marks (diamonds, triangles, etc.) correspond to different measurements.

The waveguides written are clearly too lossy for real applications (for which some authors have reported losses down to 0.1 dB/cm [47,49]), as well as not properly optimized in terms of either test wavelength and mode confinement. Here, our waveguides are used only for validating the possibility to control stress/strain and to investigate how it may influence propagation properties.

These experiments show a strong correlation between the presence of tensile stress around the laser-affected zones that supports the densification model for structures fabricated in the first regime and the ability to effectively guide light. Here, the mode size and shape are consistent with a localized increase of refractive index. Referring back to the cantilever experiments shown in Fig. 2, this further agrees with the presence of a higher material density, as demonstrated by the upward movement of the cantilevers for the same equivalent deposited energy. Again, comparing loss measurements to the cantilever experiments, we also find that the waveguide loss is minimized when the stress due to material compaction is maximized. However, the stress-state inversion does not immediately suppress the waveguiding properties. This result is important as it shows that the laser-affected zones in regime I have a more complex structure than a simple homogeneously densified volume. Indeed, if that were not the case, then the Lorentz–Lorenz relation [Eq. (3)] would predict that the refractive index contrast would simply go to zero and waveguiding would disappear in the absence of stress. This is not what we observe.

E. Interpretation and Modeling

To reconcile the two observations, we postulate the existence of a nanoporous structure (Fig. 9), also in the first regime. Pores would have a size much smaller than the visible wavelength. As the deposited energy gradually increases, the density of pores will increase as well.

In this case, the material surrounding the nanopores still has a higher refractive index than that of the bulk, thus allowing for a net increase in average refractive index in the laser-affected zone, despite an overall lower density of the material. In other words, due to the presence of these pores, the effect of densification that causes an increase of the refractive index is balanced and compensated (i.e., the net effect is that the volume variation in the laser-affected zone is zero).

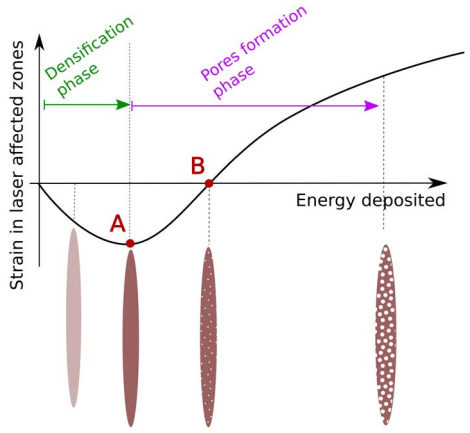

Fig. 9. Proposed phenomenological model to account for the stress-state inversion observed while increasing the energy deposited in the first regime.

Assuming a porous material, we can attempt to estimate the actual level of porosity in the material. Based on the observation of Fig. 7, we assume that the effective increase refractive index in the non-porous material, at the point where there is no volume expansion (point B in Fig. 9), is the same as when the deflection is maximum (point A in Fig. 9, i.e., where there are no pores). Assuming that the pores are much smaller than the wavelength (and that the refractive index of the pores is equal to 1, which would correspond to a gas), the rule of mixtures states

$$n_{\text{eff}}^2 = (1 - x)n_d^2 + x, \tag{6}$$

where x is the porosity, and n_d and n_{eff} are the refractive index in the densified region and the effective refractive index, respectively (we assume that the pores refractive index is 1).

On the other hand, considering the conservation of mass during laser irradiation, *at the point where no deflection is observed (point B in Fig. 9)*, the following expression holds:

$$(1 - x)\rho_{\text{densified}} + x\rho_{\text{pores}} = \rho_0, \tag{7}$$

assuming $\rho_{\text{densified}}$, the density of the material at the point of maximum deflection (i.e., assuming that at this point there is only a dense phase with no porosity). In Eq. (7), ρ_{pores} is the density of the pores and ρ_0 the density of the pristine material. Combining Eqs. (5) and (6) [and using Eqs. (1) and (2)], we finally obtain an expression of the pore density at the point of no deflection (see Fig. 6):

$$\begin{cases} x = \frac{A}{(\rho_{\text{pores}} - \rho_0) - A} \\ A = \left(\frac{3}{1+2\nu}\right)\epsilon_{\text{laz}} \\ \epsilon_{\text{LAZ}} = \left(\frac{t_{\text{sub}}}{n_{\text{lines}} X_0}\right)\frac{\delta}{2L} \end{cases}. \tag{8}$$

If we assume the pores originate from the decomposition of the silica matrix in the formation of an oxygen gas phase [37,54], ρ_{pores} is assumed to have the density of oxygen at ambient temperature (1419 kg/m^3). According to these hypothesis and using the set of Eqs. (7) fed with the actual measured data, this yields to an estimated porosity (*at the point of no deflection*) of $x = 0.98 \times 10^{-6}$, which is very low and would produce a variation of refractive index from the most densified case of about 4×10^{-7}, thus far less than the change of refractive index due to densification. It would explain why, despite the absence of "measureable" volume changes, waveguiding is still possible.

This observation has important consequences for practical waveguide writing. Indeed, this means that one can select a proper energy deposition level (approximately 6 J/mm^2 in this experiment) to achieve zero net stress outside the waveguide structures and still a sufficient refractive index increase for waveguiding.

4. CONCLUSION AND OUTLOOK

The formation of nanostructures through the process of laser–matter interaction using femtosecond lasers is, to date, not fully understood. In this study, we have revealed several key observations for the comprehension of femtosecond-laser-induced modifications in fused silica. One of the main findings of this work is that, by using a method based on the deflection of micro-cantilevers, we have demonstrated that femtosecond lasers can induce a continuous stress-state inversion in bulk fused silica.

To the best of our knowledge, this capability is quite unique in laser-induced processes. Here, stress-state inversion occurs when the structure of laser-induced modifications switch between continuously modified zones (Type I modifications) and nanograting formation (Type II modifications), but can also be achieved by increasing the deposited energy when writing in the first regime. These observations support a model where nanopores form under certain laser-exposure conditions, but are not necessarily correlated with the formation or presence of nanogratings. Whereas nanopores form when using relatively low pulse energies and deposited energy, the formation of nanogratings requires a sufficiently high field peak intensity as well as adequate energy accumulation. Furthermore, this work also demonstrates that a stress-free regime of waveguide writing can be found. This is particularly interesting for photonics applications that require the integration and combination of multiple waveguides, such as photonic lanterns [55] or quantum photonic circuits [56]. More generally, it shows that femtosecond laser exposure of silica can be used to direct-write arbitrary stress states in the volume of the material, which is of particular interest for controlling birefringence states, as well as for making mechanically reinforced parts. Finally, we suggest that the laser-affected zones formed at low energy (in the so-called regime I) has a more complex structures than one would think.

APPENDIX A

To calculate the elongation and width of the laser-affected zones, we use a simple model. The intensity at a point z along the optical axis and r perpendicular to it is given by

$$I(r,z) = I_0 \left[\frac{w_0}{w(z)}\right]^2 e^{-\frac{2r^2}{w(z)^2}}. \quad \textbf{(A1)}$$

We define the laser-affected zone as the zone such that

$$I(r,z) \geq I_t, \quad \textbf{(A2)}$$

in which I_t is a threshold intensity. This model is simplistic since it does not take into account self-focusing or other nonlinear propagation effects related to the dependence of the refractive index on the intensity. However, it provides a reasonably good approximation of the elongation and width of the laser-affected zones in the very low energy regime—which is the energy needed to produce "continuous" modifications without nanogratings. If the origin is taken in the middle of the laser-affected zone, the maximum extents of the laser-affected zones along and perpendicular to the optical axis are given by (see Fig. 2 for the definition of X_0 and Z_0)

$$Z_0 = 2\left(\frac{\pi n_\lambda w_0^2}{\lambda}\right)\sqrt{\left(\frac{I_0}{I_t} - 1\right)} \quad \text{and} \quad X_0 = 2\sqrt{\left[\frac{w_0^2}{2}\log\left(\frac{I_0}{I_t}\right)\right]}.$$

Funding. European Research Council (ERC) (ERC-2012-StG-307442); Science and Technology Facilities Council (STFC) (ST/H005595/1); Richemont International; National Basic Research Program of China (2014CB921300).

Acknowledgment. In this work, A. C. performed the cantilever experiments and the SEM observations. B. M. wrote the waveguides. S. M. and R. R. T. performed the waveguide loss measurements. C. P. did the Raman measurement. Y. B. wrote the manuscript, modeled and processed the data, and designed and supervised the research. R. R. T., Y. C., P. G., and Y. B. discussed and analyzed the results. Y. B., Y. C., and R. R. T. participated in the manuscript revisions. R. R. T. acknowledges funding from the UK STFC in the form of an STFC Advanced Fellowship (ST/H005595/1). S. M. thanks Heriot-Watt University for a James Watt Ph.D. Scholarship. The Galatea Lab (Y. B., B. M.) acknowledges sponsorship from Richemont International.

REFERENCES

1. D. Du, X. Liu, G. Korn, J. Squier, and G. Mourou, "Laser-induced breakdown by impact ionization in SiO_2 with pulse widths from 7 ns to 150 fs," Appl. Phys. Lett. **64**, 3071–3073 (1994).
2. B. C. Stuart, M. D. Feit, A. M. Rubenchik, B. W. Shore, and M. D. Perry, "Laser-induced damage in dielectrics with nanosecond to subpicosecond pulses," Phys. Rev. Lett. **74**, 2248–2251 (1995).
3. S. S. Mao, F. Quéré, S. Guizard, X. Mao, R. E. Russo, G. Petite, and P. Martin, "Dynamics of femtosecond laser interactions with dielectrics," Appl. Phys. A **79**, 1695–1709 (2004).
4. R. R. Gattass and E. Mazur, "Femtosecond laser micromachining in transparent materials," Nat. Photonics **2**, 219–225 (2008).
5. K. M. Davis, K. Miura, N. Sugimoto, and K. Hirao, "Writing waveguides in glass with a femtosecond laser," Opt. Lett. **21**, 1729–1731 (1996).
6. Y. Sikorski, A. A. Said, P. Bado, R. Maynard, C. Florea, and K. A. Winick, "Optical waveguide amplifier in Nd-doped glass written with near-IR femtosecond laser pulses," Electron. Lett. **36**, 226–227 (2000).
7. A. M. Streltsov and N. F. Borrelli, "Fabrication and analysis of a directional coupler written in glass by nanojoule femtosecond laser pulses," Opt. Lett. **26**, 42–43 (2001).
8. K. Minoshima, A. M. Kowalevicz, I. Hartl, E. P. Ippen, and J. G. Fujimoto, "Photonic device fabrication in glass by use of nonlinear materials processing with a femtosecond laser oscillator," Opt. Lett. **26**, 1516–1518 (2001).
9. R. R. Thomson, S. Campbell, I. J. Blewett, A. K. Kar, D. T. Reid, S. Shen, and A. Jha, "Active waveguide fabrication in erbium-doped oxyfluoride silicate glass using femtosecond pulses," Appl. Phys. Lett. **87**, 121102 (2005).
10. T. Meany, M. Gräfe, R. Heilmann, A. Perez-Leija, S. Gross, M. J. Steel, M. J. Withford, and A. Szameit, "Laser written circuits for quantum photonics: Laser written quantum circuits," Laser Photon. Rev. **9**, 363–384 (2015).
11. M. Beresna, M. Gecevicius, P. G. Kazansky, and T. Gertus, "Radially polarized optical vortex converter created by femtosecond laser nanostructuring of glass," Appl. Phys. Lett. **98**, 201101 (2011).
12. Y. Cheng, K. Sugioka, K. Midorikawa, M. Masuda, K. Toyoda, M. Kawachi, and K. Shihoyama, "Three-dimensional micro-optical components embedded in photosensitive glass by a femtosecond laser," Opt. Lett. **28**, 1144–1146 (2003).
13. Y. Bellouard, A. Said, M. Dugan, and P. Bado, "Monolithic three-dimensional integration of micro-fluidic channels and optical waveguides in fused silica," in *Proceedings of Materials Research Society (MRS) Symposium* (2003), Vol. **782**, pp. 63–68.
14. Y. Cheng, K. Sugioka, and K. Midorikawa, "Microfluidic laser embedded in glass by three-dimensional femtosecond laser microprocessing," Opt. Lett. **29**, 2007–2009 (2004).
15. K. Sugioka, Y. Hanada, and K. Midorikawa, "Three-dimensional femtosecond laser micromachining of photosensitive glass for biomicrochips," Laser Photon. Rev. **4**, 386–400 (2010).
16. A. Schaap, T. Rohrlack, and Y. Bellouard, "Optical classification of algae species with a glass lab-on-a-chip," Lab Chip **12**, 1527–1532 (2012).
17. F. Madani-Grasset and Y. Bellouard, "Femtosecond laser micromachining of fused silica molds," Opt. Express **18**, 21826–21840 (2010).
18. A. Schaap, Y. Bellouard, and T. Rohrlack, "Optofluidic lab-on-a-chip for rapid algae population screening," Biomed. Opt. Express **2**, 658–664 (2011).
19. Y. Bellouard, A. Said, and P. Bado, "Integrating optics and micromechanics in a single substrate: a step toward monolithic integration in fused silica," Opt. Express **13**, 6635–6644 (2005).

20. B. Lenssen and Y. Bellouard, "Optically transparent glass micro-actuator fabricated by femtosecond laser exposure and chemical etching," Appl. Phys. Lett. **101**, 103503 (2012).
21. T. Yang and Y. Bellouard, "Monolithic transparent 3D dielectrophoretic micro-actuator fabricated by femtosecond laser," J. Micromech. Microeng. **25**, 105009 (2015).
22. V. Tielen and Y. Bellouard, "Three-dimensional glass monolithic micro-flexure fabricated by femtosecond laser exposure and chemical etching," Micromachines **5**, 697–710 (2014).
23. C.-E. Athanasiou and Y. Bellouard, "A monolithic micro-tensile tester for investigating silicon dioxide polymorph micromechanics, fabricated and operated using a femtosecond laser," Micromachines **6**, 1365–1386 (2015).
24. G. Li, K. A. Winick, A. A. Said, M. Dugan, and P. Bado, "Waveguide electro-optic modulator in fused silica fabricated by femtosecond laser direct writing and thermal poling," Opt. Lett. **31**, 739–741 (2006).
25. C. B. Schaffer, J. F. García, and E. Mazur, "Bulk heating of transparent materials using a high-repetition-rate femtosecond laser," Appl. Phys. A **76**, 351–354 (2003).
26. K. Miura, J. Qiu, H. Inouye, T. Mitsuyu, and K. Hirao, "Photowritten optical waveguides in various glasses with ultrashort pulse laser," Appl. Phys. Lett. **71**, 3329–3331 (1997).
27. Y. Shimotsuma, P. G. Kazansky, J. Qiu, and K. Hirao, "Self-organized nanogratings in glass irradiated by ultrashort light pulses," Phys. Rev. Lett. **91**, 247405 (2003).
28. V. R. Bhardwaj, E. Simova, P. P. Rajeev, C. Hnatovsky, R. S. Taylor, D. M. Rayner, and P. B. Corkum, "Optically produced arrays of planar nanostructures inside fused silica," Phys. Rev. Lett. **96**, 057404 (2006).
29. F. Liang, Q. Sun, D. Gingras, R. Vallée, and S. L. Chin, "The transition from smooth modification to nanograting in fused silica," Appl. Phys. Lett. **96**, 101903 (2010).
30. Y. Liao, J. Ni, L. Qiao, M. Huang, Y. Bellouard, K. Sugioka, and Y. Cheng, "High-fidelity visualization of formation of volume nanogratings in porous glass by femtosecond laser irradiation," Optica **2**, 329–334 (2015).
31. C. Hnatovsky, R. S. Taylor, P. P. Rajeev, E. Simova, V. R. Bhardwaj, D. M. Rayner, and P. B. Corkum, "Pulse duration dependence of femtosecond-laser-fabricated nanogratings in fused silica," Appl. Phys. Lett. **87**, 014104 (2005).
32. Y. Bellouard, E. Barthel, A. A. Said, M. Dugan, and P. Bado, "Scanning thermal microscopy and Raman analysis of bulk fused silica exposed to low energy femtosecond laser pulses," Opt. Express **16**, 19520–19534 (2008).
33. Y. Bellouard, T. Colomb, C. Depeursinge, M. Dugan, A. A. Said, and P. Bado, "Nanoindentation and birefringence measurements on fused silica specimen exposed to low-energy femtosecond pulses," Opt. Express **14**, 8360–8366 (2006).
34. J. W. Chan, T. Huser, S. Risbud, and D. M. Krol, "Structural changes in fused silica after exposure to focused femtosecond laser pulses," Opt. Lett. **26**, 1726–1728 (2001).
35. A. Champion and Y. Bellouard, "Direct volume variation measurements in fused silica specimens exposed to femtosecond laser," Opt. Mater. Express **2**, 789–798 (2012).
36. J. Canning, M. Lancry, K. Cook, A. Weickman, F. Brisset, and B. Poumellec, "Anatomy of a femtosecond laser processed silica waveguide [Invited]," Opt. Mater. Express **1**, 998–1008 (2011).
37. M. Lancry, B. Poumellec, J. Canning, K. Cook, J.-C. Poulin, and F. Brisset, "Ultrafast nanoporous silica formation driven by femtosecond laser irradiation: In the heart of nanogratings," Laser Photon. Rev. **7**, 953–962 (2013).
38. A. Champion, M. Beresna, P. Kazansky, and Y. Bellouard, "Stress distribution around femtosecond laser affected zones: effect of nanogratings orientation," Opt. Express **21**, 24942–24951 (2013).
39. B. McMillen and Y. Bellouard, "On the anisotropy of stress-distribution induced in glasses and crystals by non-ablative femtosecond laser exposure," Opt. Express **23**, 86–100 (2015).
40. C. Hnatovsky, V. Shvedov, W. Krolikowski, and A. Rode, "Revealing local field structure of focused ultrashort pulses," Phys. Rev. Lett. **106**, 123901 (2011).
41. S. Hasegawa and Y. Hayasaki, "Holographic vector wave femtosecond laser processing," Int. J. Optomechatron. **8**, 73–88 (2014).
42. A. Champion, B. W. McMillen, and Y. Bellouard, "Evidence of stress-state inversion induced by non-ablative femtosecond laser pulses in fused silica," in *Bragg Gratings, Photosensitivity, and Poling in Glass Waveguides* (Optical Society of America, 2014), paper JM5A–33.
43. S. Rajesh and Y. Bellouard, "Towards fast femtosecond laser micromachining of fused silica: the effect of deposited energy," Opt. Express **18**, 21490–21497 (2010).
44. Y. Bellouard, A. Said, M. Dugan, and P. Bado, "Fabrication of high-aspect ratio, micro-fluidic channels and tunnels using femtosecond laser pulses and chemical etching," Opt. Express **12**, 2120–2129 (2004).
45. G. G. Stoney, "The tension of metallic films deposited by electrolysis," Proc. R. Soc. London A **82**, 172–175 (1909).
46. S. Timoshenko, "Analysis of bi-metal thermostats," J. Opt. Soc. Am. **11**, 233–255 (1925).
47. P. Bado, A. A. Said, M. Dugan, and T. Sosnowski, "Dramatic improvements in waveguide manufacturing with femtosecond lasers," in *National Fiber Optic Engineers Conference (NFOEC)* (2002), Vol. **2**, pp. 1153–1158.
48. P. Bado, A. A. Said, M. A. Dugan, and T. Sosnowski, "Waveguide fabrication methods and devices," U.S. patent 7,391,947 (June 24, 2008).
49. Y. Nasu, M. Kohtoku, and Y. Hibino, "Low-loss waveguides written with a femtosecond laser for flexible interconnection in a planar light-wave circuit," Opt. Lett. **30**, 723–725 (2005).
50. Y. Okamura, S. Yoshinaka, and S. Yamamoto, "Measuring mode propagation losses of integrated optical waveguides: a simple method," Appl. Opt. **22**, 3892–3894 (1983).
51. C. Fiori and R. A. B. Devine, "Evidence for a wide continuum of polymorphs in a-SiO_2," Phys. Rev. B **33**, 2972–2974 (1986).
52. R. E. Schenker and W. G. Oldham, "Ultraviolet-induced densification in fused silica," J. Appl. Phys. **82**, 1065–1071 (1997).
53. H. Kakiuchida, K. Saito, and A. J. Ikushima, "Refractive index, density and polarizability of silica glass with various fictive temperatures," Jpn. J. Appl. Phys. **43**, L743 (2004).
54. H. Sun, S. Juodkazis, and M. Watanabe, "Generation and recombination of defects in vitreous silica induced by irradiation with a near-infrared femtosecond laser," J. Phys. Chem. B **104**, 3450–3455 (2000).
55. R. R. Thomson, T. A. Birks, S. G. Leon-Saval, A. K. Kar, and J. Bland-Hawthorn, "Ultrafast laser inscription of an integrated photonic lantern," Opt. Express **19**, 5698–5705 (2011).
56. G. D. Marshall, A. Politi, J. C. F. Matthews, P. Dekker, M. Ams, M. J. Withford, and J. L. O'Brien, "Laser written waveguide photonic quantum circuits," Opt. Express **17**, 12546–12554 (2009).